https://doi.org/10.37434/tpwj2021.05.07

ANALYSIS OF THE PROPERTIES OF ELECTRON BEAM WELDED JOINTS OF ALUMINIUM LITHIUM ALLOY LATEST GENERATION

Mir. Sahul[1], **Mar. Sahul**[2], **L. Čaplovič**[2], **M. Marônek**[1], **I. Klochkov**[3] and **S. Motrunich**[3]
[1]Slovak University of Technology in Bratislava, Faculty of Materials Science and Technology in Trnava,
Department of Welding and Joining of Materials
J. Bottu 25, 917 24 Trnava, Slovakia. E-mail: miroslav.sahul@stuba.sk
[2]Slovak University of Technology in Bratislava, Faculty of Materials Science and Technology in Trnava,
Institute of Materials Science
J. Bottu 25, 917 24, Trnava, Slovakia
[3]E.O. Paton Electric Welding Institute of the NAS of Ukraine
11 Kazymyr Malevych Str., 03150, Kyiv, Ukraine. E-mail: office@paton.kiev.ua

Electron beam welded joints made on AW2099 aluminium lithium alloy with the thickness of 4 mm were analysed. The third generation of aluminium lithium alloys was developed to improve the drawbacks of the second one. Various electron beam welding parameters (beam current, welding speed) were tested. Accelerating voltage was constant, i.e., 55 kV. Defect free welded joints were produced under optimized welding parameters. Weld metal microstructure and welded joints mechanical properties were investigated. Microstructure of weld metal matrix consists of α-aluminium solid solution. Inter-dendrite areas were enriched in alloying elements due to segregation. Narrow equiaxed zone was observed at the location close to the fusion boundary being characteristic for welded joints made on aluminium lithium alloys. The character of the grains changed in the direction towards weld metal centre to columnar dendritic and equiaxed dendritic. Microhardness values reduction in the weld metal was observed which is associated to the dissolution of strengthening precipitates. 19 Ref., 1 Table, 9 Figures.

Keywords: AW2099 aluminium lithium alloy, electron beam welding, equiaxed zone, scanning electron microscopy, drop of microhardness

Aluminium lithium alloys have received extensive attention in aerospace industry due to low density, high strength/weight ratio, high Young's modulus, improved fatigue crack growth resistance and resistance to corrosion. It is known that adding of 1 % of lithium resulted in the decrease in density by 3 % and improvement in Young's modulus by 6 % [1–7].

The third generation of aluminium lithium alloys was developed to remove the disadvantages of previous generation. Important representatives of newly developed alloys are 2099 and 2199 being applied in the fuselage's skin stringer components [8]. Al–Li alloys of the new generation are characteristic by higher Cu/Li ratio than previous generation [9]. The application of 2099 alloy caused the reduction of weight of wing components by 14 % and cryogenic tanks by 21 % [10].

Currently, worldwide research focuses on the welding of aluminium lithium alloys. Friction stir welding belongs to the possible joining methods [11–18]. The main issues when fusion welding of these alloys is carried out are porosity, hot cracking, evaporation of alloying elements and decrease in mechanical properties. Drop in mechanical properties is associated with the dissolution of strengthening precipitates due to thermal cycle of welding. From this point of view, the application of low heat input electron beam welding could be more convenient. High welding speeds lead to formation of minimum deformations and residual stresses. Furthermore, narrower weld metal and HAZ represents softening region of much smaller dimensions in comparison to conventional arc welding processes [19, 20].

Only a few papers focus on the electron beam weldability of AW2099 aluminium lithium alloy have been published. The purpose of the paper is to analyse the properties of electron beam welded joints made on latest generation AW2099 aluminium lithium alloy.

Materials and methods. AW2099 aluminium lithium alloy, 4 mm thick, was suggested as experimental material. Initial thickness of as delivered alloy

Mir. Sahul — https://orcid.org/0000-0001-5091-6381, Mar. Sahul — https://orcid.org/0000-0001-9472-500X,
L. Čaplovič — https://orcid.org/0000-0002-2280-008X, M. Marônek — https://orcid.org/0000-0002-4716-8092,
I. Klochkov — https://orcid.org/0000-0001-6490-8905, S. Motrunich — https://orcid.org/0000-0002-8841-8609

Chemical composition of AW2099 aluminium lithium alloy

Cu	Li	Zn	Mg	Mn	Zr	Ti	Fe	Si	Be	others	Al
2.7	1.8	0.70	0.30	0.30	0.09	0.10	0.07	0.05	0.0001	0.03	Bal.

was 25.4 mm. The thickness of AW2099 alloy was reduced to 4 mm. Solution annealing at 530 °C/1 hr. was carried out before hot rolling. The chemical composition of the AW 2099 alloy provided by Smiths High Performance is given in Table.

PZ EZ 30 STU electron beam welding machine from First Welding Company, Inc. in Bratislava with the maximum accelerating voltage of 60 kV was used for manufacturing of welded joints (Figure 1). The maximum beam current 500 mA and output power are 30 kW. Welded joints were produced in the Centre of Excellence of 5-axis Machining (CE5AM) of the Faculty of Materials Science and Technology in Trnava, Slovakia. The vertical electron beam welding was carried out within experiments. The volume of vacuum chamber is 14.3 m^3. The vacuum level during welding was 10^{-2} Pa. Accelerating voltage of 55 kV and focusing current of 885 mA were used.

After metallographic preparation, the samples were etched with Keller's reagent (chemical composition 1 ml HF + 1.5 ml HCl + 2.5 ml HNO_3 + 95 ml distilled H_2O). High resolution field emission gun scanning electron microscope JEOL JSM 7600 F with EDS analyser X-max 50 mm^2 of Oxford Instruments was used to identify elemental distribution across investigated location. Microhardness measurements across base metal–HAZ–weld metal interface was carried out on Buehler IndentaMet 1100™ Series microhardness tester. The parameters of measurements were as follows: loading force 0.98 N, dwell time 10 s. Distance between indents in base metal and HAZ was 100 and 500 μm within the weld metal.

Results. Effect of welding parameters on the weld bead appearance and weld defects is given in Figure 2. When beam current of 50 mA was used, the application of welding speeds up to 20 mm/s resulted in the drop through. The heat input was too high in such cases. Increasing the welding speed to 30 mm/s resulted in the elimination of mentioned burn through. On the other hand, slight undercut was observed. Increase of beam current to 60 and 70 mA (at welding speed of 30 mm/s) resulted in solidification cracking. Smooth surface without weld defects was observed when lower heat inputs were applied. Beam currents 60 and 65 mA and welding speeds from 50 to 80 mm/s resulted in the production of defect-free welded joints with smooth surface.

Microstructure of weld metal–heat affected zone interface (welded joint produced with beam current of 50 mA and welding speed of 30 mm/s) is given in Figure 3. The equiaxed zone (EQZ) was observed close to the fusion boundary. Equiaxed grains were probably formed due to heterogeneous nucleation at the lithium and zirconium rich precipitates.

In the direction towards weld center, the change in the dendrite morphology was observed. Columnar dendrite zone and equiaxed dendrite zone were found. The width of EQZ of about 20 μm consisting of equiaxed grains of average size 7 μm was documented between the fusion boundary and weld metal. Wang et al. observed that the grain volume was without precipitates and similarly found eutectics at the EQZ boundaries [11].

Chen et al. found EQZ in the un-fused region in the welded joints produced by newly developed fusion-diffusion electron beam welding of 2195-T3 aluminium lithium alloy. The diameter of equi-axed crystals was 50 μm. Weld metal and EQZ were characteristic by the presence of Al_2Cu and T1 precipitates [21].

Figure 1. PZ EZ 30 STU electron beam welding machine

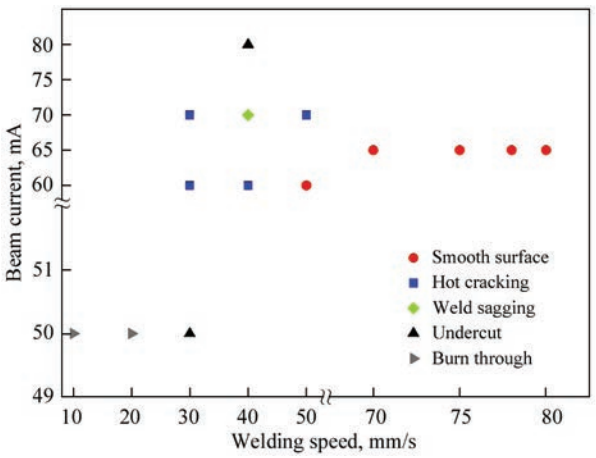

Figure 2. Effect of welding parameters on bead appearance and type of weld defects

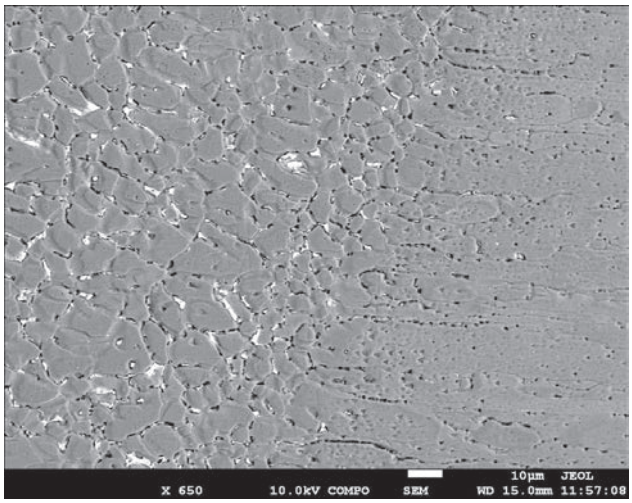

Figure 3. Microstructure of weld metal–HAZ interface (I_B = = 50 mA, v = 30 mm/s)

The microstructure of HAZ–weld metal interface of welded joint produced with lower heat input 45 J/mm (beam current of 65 mA and welding speed of 80 mm/s) is documented in Figure 4. Lower heat input caused that the width of EQZ decreased to about 10 μm and was non-uniform across weld depth. EQZ is formed in some locations along fusion boundary only by one grain.

The weld root area of welded joint produced with the beam current of 60 mA and welding speed of 50 mm/s is given in Figure 5. The structure has a typical casting character, with a dendritic morphology. The matrix is formed by a α-solid solution of alloying elements Cu and Li in aluminium and at the inter-dendrite locations depending on the maximum temperature and holding, the precipitation of secondary phases δ′-Al_3Li, β′-Al_3Zr, θ-Al_2Cu could be expected.

Inter-dendrite precipitate documented by electron microscopy is given in Figure 6. EDS «linescan» across aluminium matrix–precipitate–aluminium matrix interface is given in Figure 7. The increase in copper, iron, and manganese content was observed in the

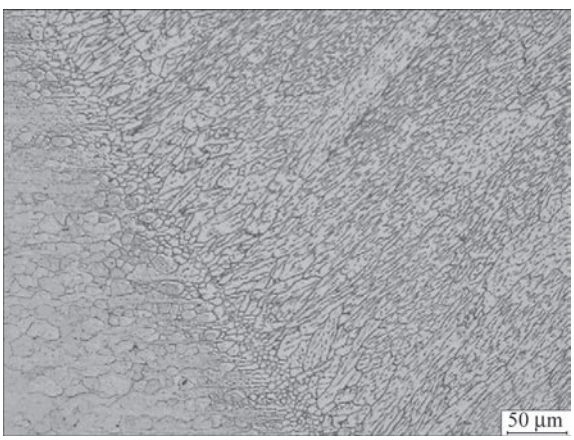

Figure 4. Microstructure of HAZ–weld metal interface (I_B = = 65 mA, v = 80 mm/s)

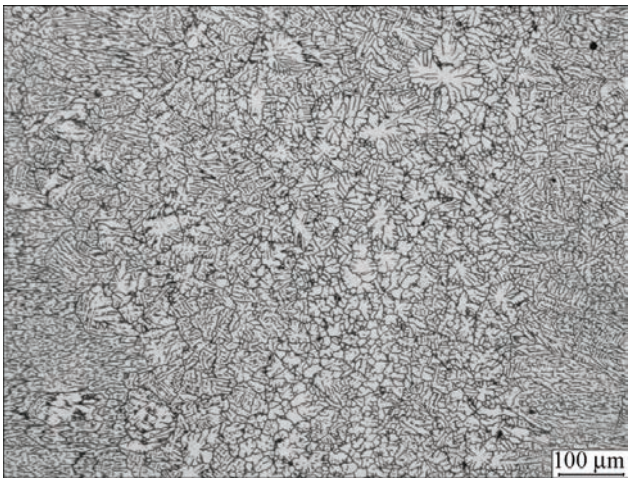

Figure 5. The microstructure of the equiaxed dendrite zone in the weld metal centre (I_B = 60 mA, v = 50 mm/s)

site where precipitate is present. On the other hand, aluminium content remarkably decreased.

The course of microhardness across welded joints interfaces are given in Figure 8. The average microhardness of base material was 109 *HV*0.1. Welded joint produced with beam current of 50 mA and welding speed of 30 mm/s, i.e., heat input 92 J/mm was characterized by drop of microhardness in the weld metal. The average microhardness measured in the weld metal is about 75 *HV*0.1, representing about 69 % of the microhardness of the base material.

Microhardness trend for welded joint produced with higher heat input, following welding parameters: beam current 80 mA and welding speed of 40 mm/s is given in Figure 9. The calculated heat input is 110 J/mm. Similarly, the drop of microhardness was recorded in the weld metal. The averaged microhardness reached the value of 81 *HV*0.1 being about 74 % of the averaged values measured in the AW2099 aluminium lithium alloy.

Chen et al. investigated the reasons for lower mechanical properties of electron beam welded joints on 2195-T3 aluminium lithium alloy with the thickness of 5 mm. Similarly, authors also observed the decrease in the hardness in the welded joint averaging

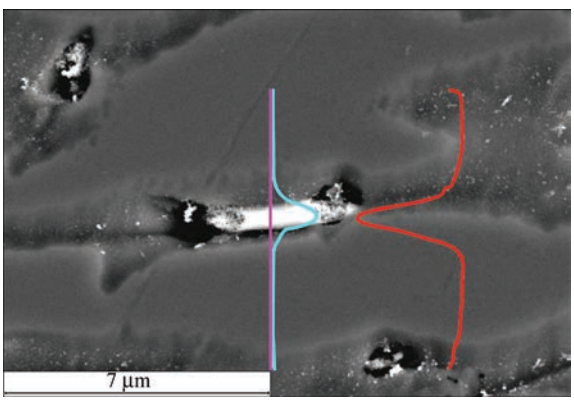

Figure 6. Inter-dendrite precipitate in the weld metal

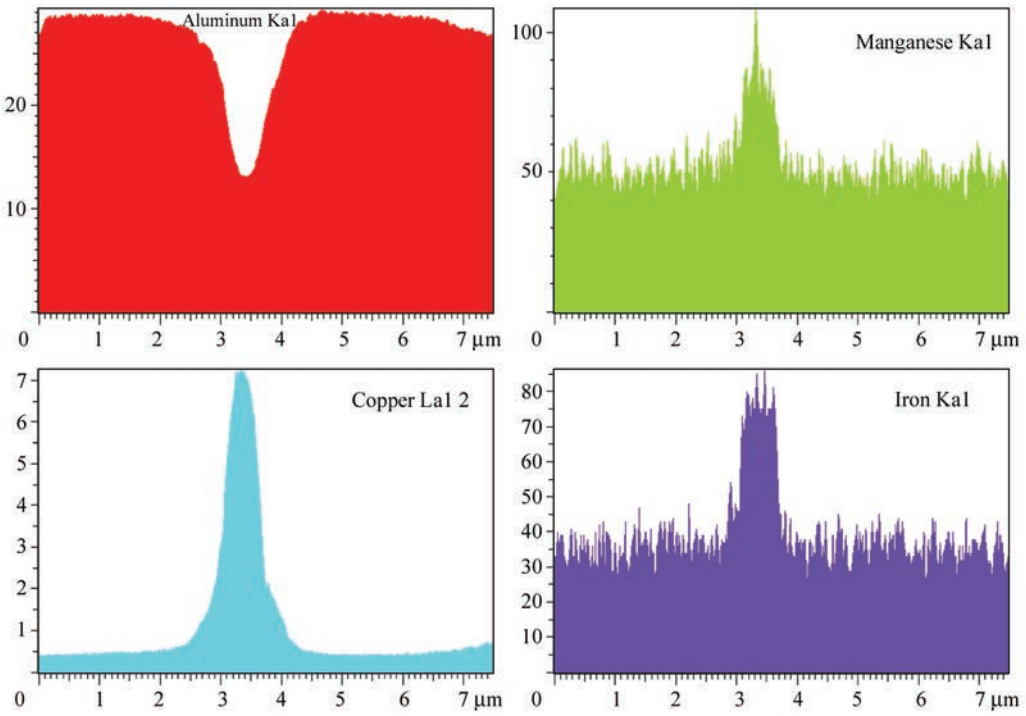

Figure 7. Course of aluminium, copper, manganese and iron across dendrite boundary (the value on the ordinate axis must be increased 1000 times)

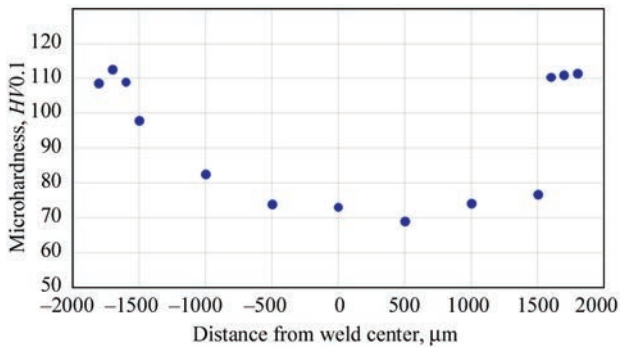

Figure 8. The course of microhardness across welded joint produced by beam current 50 mA and welding speed 30 mm/s

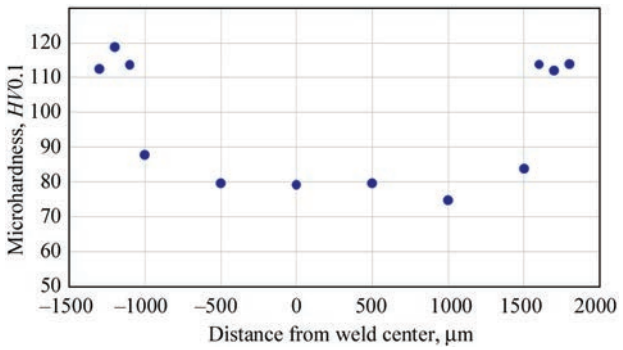

Figure 9. The course of microhardness across welded joint produced by beam current 80 mA and welding speed 40 mm/s

72 *HV*, representing about 60 % of the base materials hardness [22].

Based on the course of the measured values of microhardness, it can be stated that the microhardness of the weld metal decreased in comparison to the base material. Due to the thermal influence of the material by the welding thermal cycle, main precipitates T1 (Al_2CuLi), most significantly contributing to the increase of mechanical properties during the heat treatment of mentioned aluminium alloy dissolved in the weld metal region. Reheating and melting of the base material resulted in the dissolution of phase T1.

Conclusions

The following could be concluded according to the results attained by the analysis of the electron beam welded joints made on AW2099 aluminium lithium alloy:

■ electron beam welding of latest generation aluminium lithium led to the production of sound joints by optimization of welding parameters;

■ higher heat input resulted in burn through and formation of solidification cracking;

■ non-dendritic equiaxed zone was observed in the location close to the fusion boundary;

■ the width of EQZ decreased when lower heat input was used;

■ increase in the copper content was observed at the inter-dendrite areas due to segregation;

■ decrease in average microhardness of weld metal was found and it was probably caused by dissolution of precipitates.

Acknowledgement. *This work was supported by the Slovak Research and Development Agency under the contract No. APVV-15-0337.*

The paper was prepared under the support of the KEGA cultural and educational grant agency of the Ministry of Education, Science, Research, and Sport of the Slovak Republic, project No. 001STU-4/2019.

This publication was supported by the Operational Programme Research and Innovation for the project: Scientific and Research Centre of Excellence SlovakION for Material and Interdisciplinary Research, code of the project ITMS2014+:313011W085 co-financed by the European Regional Development Fund.

The work was carried out also within the framework of the departmental order programme of the National Academy of Sciences of Ukraine by E.O. Paton Electric Welding Institute (basic research no.6541230) titled «Supporting Development of the Priority Research Areas».

1. Xiao, R., Zhang, X. (2014) Problems and issues in laser beam welding of aluminum-lithium alloys. *J. Materials. Proc. Technology*, **16**, 166–175.
2. Gao, Ch., Gao, R., Ma, Y. (2015) Microstructure and mechanical properties of friction spot welding aluminium-lithium 2A97 alloy. *Mater. Des.*, **83**, 719–727.
3. Han, B., Tao, W., Chen, Y., Li, H. (2017) Double-sided laser beam welded T-joints for aluminium-lithium alloy aircraft fuselage panels: Effects of filler elements on microstructure and mechanical properties. *Opt. Laser Technol*., **93**, 99–108.
4. Lee, H.-S., Yoon, J.-H., Yoo, J.-T., No, K. (2016) Friction stir welding process of aluminum-lithium alloy 2195. *Procedia Eng*., **149**, 62–66.
5. Ma, Y.E., Xia, Z.C., Jiang, R.R., Li, W.Y. (2013) Effect of welding parameters on mechanical and fatigue properties of friction stir welded 2198 T8 aluminum-lithium alloy joints. *Eng. Fract. Mech*., **114**, 1–11.
6. Zhang, F., Shen, J., Yan, X.-D. et al. (2014) Homogenization heat treatment of 2099 Al–Li alloy. *Rare Met*., **33**, 28–36.
7. Tao, Y., Ni, D.R., Xiao, B.L. et al. (2017) Origin of unusual fracture in stirred zone for friction stir welded 2198-T8 Al–Li alloy joints. *Mater. Sci. Eng*., A **693**, 1–13.
8. Rajan, R., Kah, P., Mvola, B., Martikainen, J. (2016) Trends in aluminium alloy development and their joining methods. *Rev. Adv. Mater. Sci*., **44**, 383–397.
9. Dursun, T., Soutis, C. (2014) Recent developments in advanced aircraft aluminium alloys. *Mater. Des*., **56**, 862–871.
10. Romios, M., Tiraschi, R., Ogren, J.R., Babel, H.W. (2005) Design of multistep aging treatments of 2099 (C458) Al–Li alloy. *J. Mater. Eng. Perform*., **14**, 641–646.
11. Wang, G., Zhao, Y., Hao, Y. (2018) Friction stir welding of high-strength aerospace aluminium alloy and application in rocket tank manufacturing. *J. of Mater. Sci. and Technology*, **34**, 73–91.
12. Poklyatsky, A.G., Knysh, V.V., Klochkov, I.N., Motrunich, S.I. (2016) Features and advantages of the process of friction stir welding of butt joints of sheet aluminium-lithium alloys. *The Paton Welding J*., **6**, 93–98.
13. Milagre, M.X., Mogili, N.V., Donatus, U. et al. (2018) On the microstructure characterization of the AA2098-T351 alloy welded by FSW. *Mater. Charact.*, **140**, 233–246, DSC vyzera byt fajn.
14. Li, W.Y., Chu, Q., Yang, X.W. et al. (2018) Microstructure and morphology evolution of probeless friction stir spot welded joints of aluminum alloy. *J. of Materials Proc. Technology*, **252**, 69–80.
15. Knysh, V.V., Klochkov, I.M., Motrunich, S.I., Poklyatsky, A.G. (2021)Influence of irregular cyclic load on fatigue resistance of thinsheet welded joints of heat-strengthened aluminium alloys. *The Paton Welding J.*, **1**, 9–13.
16. de Castro, C.C., Plaine, A.H., Dias G.P. et al. (2018) Investigation of geometrical features on mechanical properties of AA2198 refill friction stir spot welds. *J. Manuf. Processes*, **36**, 330–339.
17. Hatamleh, O., Rivero, I.V., Swain S.E. (2009) An investigation of the residual stress characterization and relaxation in peened friction stir welded aluminium-lithium alloy joints. *Mater. Des*., **30**, 3367–3373.
18. Motrunich, S., Klochkov, I., Poklaytsky, A. (2020)High cycle fatigue behaviour of thin sheet joints of aluminium-lithium alloys under constant and variable amplitude loading. *Weld World*, **64**, 1971–1979.
19. Weglowski, M.St., Blacha, S., Phillips, A. (2016) Electron beam welding — Techniques and trends — Review. *Vacuum*, **130**, 72–92.
20. Cui, L., Li, X., He, D. et al. (2012) Effect of Nd:YAG laser welding on microstructure and hardness of an Al–Li based alloy. *Mater. Charact*., **71**, 95–102.
21. Chen, G., Yin, Q., Zhang, G., Zhang, B. (2020) Fusion-diffusion electron beam welding of aluminium-lithium alloy with Cu nano-coating. *Mater. Des*., **188**, 108439.
22. Chen, G., Yin, Q., Zhang, G., Zhang, B. (2020) Underlying causes of poor mechanical properties of aluminum-lithium alloy electron beam welded joints. *J. Manuf. Process*., **50**, 216–223.

Received 22.03.2021

MAY 15, 2006 Cloud Gate sculpture was opened. It is located in the business quarter of Chicago, USA. Its author is the Indian-born British artist Anish Kapoor (born in 1954). The sculpture consists of 168 stainless steel plates, welded together and polished so well that its exterior has no visible welds. The dimensions of the sculpture are 10 (height), 20 (length) and 13 (width) m, its weight is about 100 t. Welders used hybrid laser-arc welding. Cloud Gate is one of the most famous and recognizable monuments of our time. It is believed that the sculpture form was inspired by a mercury drop.

MAY 22, 2012 Opening of Tokyo Skytree — TV tower in Sumida district (Tokyo, Japan). It is the world's tallest TV tower of 634 m height and the second in height construction in the world after «Burge-Halifa». The entire structure of the tower consists of «lattice» elements, each of which is a combination of triangles, as part of other components. These elements are connected through branch joints and pipes. All the structures are joined by welding directly to the main support, without application of any other fastening systems or methods. This type of connection has a very simple appearance and high seismic resistance.